Adsorption (2014) 20:213–223
DOI 10.1007/s10450-013-9588-2

Fluids in nanospaces: molecular simulation studies to find out key mechanisms for engineering

Minoru T. Miyahara · Ryohei Numaguchi · Tatsumasa Hiratsuka · Kazuyuki Nakai · Hideki Tanaka

Received: 11 July 2013 / Accepted: 4 October 2013 / Published online: 15 October 2013

Abstract We have analyzed various phenomena that occur in nanopores, focusing on elucidating their key mechanisms, to advance the effective engineering use of nanoporous materials. As ideal experimental systems, molecular simulations can effectively provide information at the molecular level that leads to mechanistic insight. In this short review, several of our recent results are presented. The first topic is the critical point depression of Lennard-Jones fluid in silica slit pores due to finite size effects, studied by our original Monte Carlo (MC) technique. We demonstrate that the first layers of adsorbed molecules in contact with the pore walls act as a "fluid wall" and impose extra finite size effects on the fluid confined in the central portion of the pore. We next present a new kernel for pore size distribution (PSD) analysis, based entirely on molecular simulation, which consists of local isotherms for nitrogen adsorption in carbon slit pores at 77 K. The kernel is obtained by combining grand canonical Monte Carlo (GCMC) method and open pore cell MC method that was developed in the previous study. We show that overall trends of the PSDs of activated carbons calculated with our new kernel and with conventional kernel from non-local density functional theory are nearly the same; however, apparent difference can be seen between them. As the third topic, we apply a free energy analysis method with the aid of GCMC simulations to investigate the gating behavior observed in a porous coordination polymer, and propose a mechanism for the adsorption-induced structural transition based on both the theory of equilibrium and kinetics. Finally, we construct an atomistic silica pore model that mimics MCM-41, which has atomic-level surface roughness, and perform molecular simulations to understand the mechanism of capillary condensation with hysteresis. We calculate the work required for the gas–liquid transition from the simulation data, and show that the adsorption branch with hysteresis for MCM-41 arise from spontaneous capillary condensation from a metastable state.

Keywords Fluids in nanospaces · Critical point depression · Pore size distribution · Porous coordination polymers · Capillary condensation

M. T. Miyahara (✉) · R. Numaguchi · T. Hiratsuka · H. Tanaka
Department of Chemical Engineering, Kyoto University, Katsura, Nishikyo, Kyoto 615-8510, Japan
e-mail: miyahara@cheme.kyoto-u.ac.jp

K. Nakai
BEL Japan, Inc., 1-9-1, Harada-naka, Toyonaka, Osaka 561-0807, Japan

1 Introduction

Over the last two decades, molecular simulations have played an important role in the understanding of the phase behaviors of confined fluids in nanopores (Gelb et al. 1999; Gubbins et al. 2010, 2011; Coasne et al. 2013). Molecular simulations can provide a fundamental understanding of experimentally observed adsorption phenomena, and can also be used to gain detailed information at the molecular level that may not be obtained by experiment. We have studied various adsorption phenomena in nanopores, elucidating key mechanisms and constructing thermodynamic models, which should lead to the effective engineering use of nanoporous materials (Miyahara and Gubbins 1997; Miyahara et al. 1997, 2000a, b; Kanda et al. 2004; Kanda and Miyahara 2007; Watanabe et al. 2009; Sugiyama et al. 2012; Numaguchi et al. 2013; Tanaka et al. 2013; Miyahara

and Tanaka 2013). Molecular simulations are quite effective because they can provide *ideal experimental systems* through which to confirm the thermodynamic models. This paper is an introduction and overview of our recent simulation studies for adsorption engineering.

Phase behaviors of confined fluids are dramatically different from those of bulk fluids, and an understanding of these anomalous behaviors is important for the development of new technologies for industry. In particular, the determination of critical properties is integral to the calculation and modeling of phase equilibria, yet few studies have been reported for the case of confined fluids (Mon and Binder 1992; Vishnyakov et al. 2001; Shi et al. 2002; Jana et al. 2009; Liu et al. 2010; Singh and Singh 2011). Therefore, following our previous work to determine phase boundaries in nanopores (Miyahara and Gubbins 1997, 2000b; Kanda and Miyahara 2007; Miyahara and Tanaka 2013), the critical points of Lennard-Jones (LJ) fluid in silica slit pores were studied with a molecular simulation cell, which holds gas–liquid coexisting conditions yet possesses the ability to estimate its chemical potential. We also employed "fluid" slit pores whose walls consisted of LJ fluid, and show that the attractive pore wall of a silica slit pore provides anomalous finite size effects on the critical properties of the confined fluid by comparing both phase equilibria in the silica and "fluid" slit pores.

Nanopore-size characterization requires an accurate kernel consisting of a large number of local isotherms for various pore sizes, which are to be obtained, desirably, by molecular simulations. At present, however, kernels obtained by non-local density functional theory (NLDFT) are predominantly used (Ravikovitch et al. 1995; Olivier 1995; Ravikovitch et al. 1998, 2000, 2001; Do and Do 2003; Neimark et al. 2009; Jagiello and Olivier 2013) because of the high computational costs for molecular simulations in general. Therefore, by extending our earlier work (Miyahara et al. 1997), we developed an open pore cell combined with the Monte Carlo technique (open pore cell MC method) to satisfy two requirements: to avoid metastable states or hysteresis loops, and to determine equilibrium transition pressures easily without heavy computational loads (Miyahara and Tanaka 2013). In this paper, we present a new kernel consisting of local isotherms for nitrogen adsorption in carbon slit pores at 77 K obtained by combining the grand canonical Monte Carlo (GCMC) method and the open pore cell MC method, and compare the pore size distributions of activated carbons calculated with both our new kernel and the conventional NLDFT kernel.

Porous coordination polymers (PCPs), also known as metal–organic frameworks (MOFs), are a new class of porous materials which have prominent physicochemical properties (Kitagawa et al. 2004; Rowsell and Yaghi 2004; Rosseinsky 2004; Horike et al. 2009). In particular, PCPs with flexible frameworks show a peculiar adsorption behavior known as a gating or breathing phenomenon: at a certain pressure, guest molecules adsorb or desorb abruptly, accompanied by the deformation of the host framework. This stimulus-responsive behavior should be useful for various applications such as gas storage (Düren et al. 2004; Kanoh et al. 2009); separation (Düren and Snurr 2004; Nakagawa et al. 2010), molecular sensing (Yanai et al. 2011), and drug delivery systems (Horcajada et al. 2006). For the practical use of PCPs, a fundamental understanding of the mechanism of the adsorption-induced structural transition is absolutely required, and molecular simulation should play a crucial role in that determination. However, direct simulation of the gating behavior remains challenging because of the long-lived metastability of the structural transition. Our approach for overcoming this difficulty is to use the thermodynamic integration method to obtain the free energy landscape of the system under various settings of pressure by the GCMC method (Watanabe et al. 2009; Sugiyama et al. 2012; Numaguchi et al. 2013). We applied this free energy analysis method to a stacked-layer PCP for which the gating transition was observed experimentally (Li and Kaneko 2001; Kitaura et al. 2003; Noguchi et al. 2005; Kondo et al. 2006; Kanoh et al. 2009), and propose a mechanism for the adsorption-induced structural transition based on both the theory of equilibrium and the kinetics.

Siliceous mesoporous materials such as MCM-41 and SBA-15 have attracted much attention because of their potential uses as catalyst supports, in separation, in drug delivery, and so forth. Recent theoretical studies and simulations have shown that the surface roughness of the pore walls affects the adsorption and capillary condensation of gases, and it is essential for representing the adsorption isotherms for siliceous mesoporous materials (Coasne and Pellenq 2004a, b; Sonwane et al. 2005; Coasne et al. 2006a, b, 2007, 2008a, b, 2010; Coasne and Ugliengo 2012). However, a clear understanding of the mechanism of adsorption hysteresis relevant to capillary condensation is still lacking. Therefore, we constructed an atomistic silica pore model mimicking MCM-41, which has molecular-level surface roughness, and performed molecular simulations to understand the mechanism of capillary condensation with hysteresis. We calculated the canonical work function with the simulation data, which is the work required for the gas–liquid transition according to Neimark and Vishnyakov (2006), and show that the adsorption branch with hysteresis derives from spontaneous capillary condensation.

2 Critical points in nanopores

We employed a slit-like pore cell with a high aspect ratio of pore length to width, in order to maintain gas–liquid

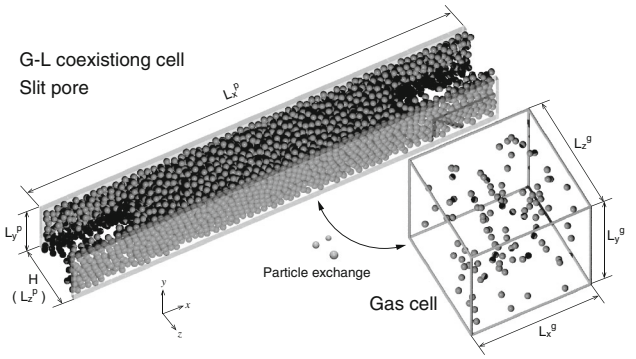

Fig. 1 Schematic representations of the simulation cells used in the G–L coexisting cell method

coexistence in the pore, and combined it with a gas cell to measure the chemical potential of the system (G–L coexisting cell method), similar to the gauge cell method (Neimark and Vishnyakov 2000). Our system, with the two simulation cells developed for this study, is shown in Fig. 1. The system was steadily led to a thermodynamically stable state by forming concave menisci in the pore cell, when the system contained a sufficient number of particles. The choice of the size of the gas cell was straightforward, unlike the gauge cell method, in which the size must be chosen to meet a particular condition (Neimark and Vishnyakov 2000).

The Lennard-Jones (LJ) potential, with the parameters $\sigma_{ff} = 0.3615$ nm and $\varepsilon_{ff}/k_B = 101.5$ K (k_B is the Boltzmann constant), and a cut-off radius of $5\sigma_{ff}$ were used as the fluid–fluid interactions of nitrogen. In this study, we assumed two kinds of pore walls; one was silica and the other was a solid with the density and interaction parameters of liquid nitrogen at 77 K (hereafter, a silica slit pore and a fluid slit pore). The slit pores were modeled by two walls with width H, where H was defined as the distance between the layers as measured from the atomic centers at the surfaces. The Steele's 10-4 potential was employed for the solid–fluid interaction potential between a LJ nitrogen and one silica layer:

$$\phi(z) = 2\pi\rho_s\varepsilon_{sf}\sigma_{sf}^2\left[\frac{2}{5}\left(\frac{\sigma_{sf}}{z}\right)^{10} - \left(\frac{\sigma_{sf}}{z}\right)^{4}\right] \quad (1)$$

where ρ_s is number density of atoms in the layer, and σ_{sf} and ε_{sf} are the LJ parameters. Then, in the case of the fluid slit pore, the pore wall was assumed to be a slab consisting of five layers with interlayer distances of Δ as:

$$\phi(z) = 2\pi\rho_s\varepsilon_{sf}\sigma_{sf}^2\sum_{i=0}^{4}\left[\frac{2}{5}\left(\frac{\sigma_{sf}}{z+i\Delta}\right)^{10} - \left(\frac{\sigma_{sf}}{z+i\Delta}\right)^{4}\right] \quad (2)$$

where $\rho_s/\Delta = 17.3$ nm^{-3} is the density of liquid nitrogen at 77 K. The solid–fluid cross interaction parameters were calculated with the Lorentz-Berthelot mixing rules, and those used for the silica and fluid slit pores are tabulated in Table 1.

Table 1 Parameters for the solid–fluid intermolecular potentials

Wall	σ_{sf} (nm)	ε_{sf}/k (K)	ρ_s (nm^{-2})	Δ (nm)
Silica	0.317	147	153	–
Fluid	0.3615	101.5	7.01	0.406

The total interaction potential for a LJ nitrogen in the silica and fluid slit pores was obtained by adding the contributions from each wall as:

$$\Phi(z) = \phi(z) + \phi(H - z) \quad (3)$$

Periodic boundary conditions in the x and y directions were applied for the pore cell, and the lateral dimensions of the cell were set as $L_x^p = 70\ \sigma_{ff}$ and $L_y^p = 10\ \sigma_{ff}$. Then, the size of the gas cell was changed from $L_x^g = L_y^g = L_z^g = 27\ \sigma_{ff}$ to $11\ \sigma_{ff}$, depending on the system temperature, to reduce the total number of particles and the computational costs.

In analogy with the gauge cell method, two trial moves were performed in our G–L coexisting cell method: displacement of a randomly selected particle and transfer of a particle selected at random from one cell to the other. The probabilities of the two trial moves were set to be equal. A single simulation run for a system temperature was performed for 1×10^4 MC steps per particle to achieve equilibrium, after which the average properties were collected for another 2×10^4 MC steps per particle. The gas and liquid densities in the pore were obtained from the central portion of the pore cell to eliminate the contributions from the densely packed first and second layers of adsorbed molecules. Then, as the system approaches the critical point, the adsorbed phase undergoes substantial density fluctuation, and the vapor–liquid meniscus becomes ill-defined. To deal with this problem, we maintained the center of mass of the whole adsorbed phase along the x axis over the center of the adsorption cell during the simulation. The center of mass of the adsorbed phase along the x axis was calculated by summing x coordinates of all the fluid particles, and the x coordinate of the center of mass was subtracted from those of all the fluid particles. This procedure makes it possible to obtain the gas and liquid densities by sampling the number of fluid particles at the both ends and the center of the adsorption cell.

Figures 2 and 3 show the phase diagrams of the confined nitrogen fluid in the silica and fluid slit pores as a function of the slit pore width, determined by the G–L coexisting cell method. The critical parameters were estimated with the coexistence densities by the least squares fitting of the scaling law and the rectilinear law. The obtained reduced

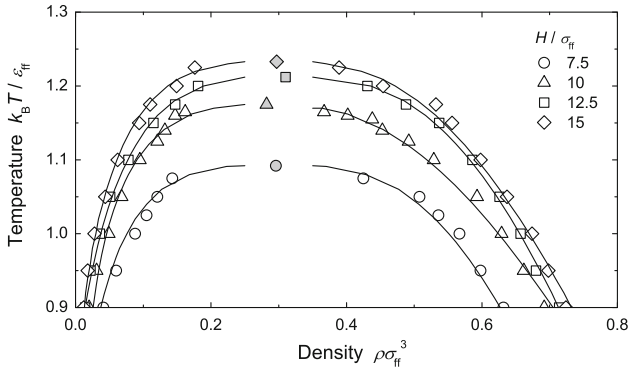

Fig. 2 Phase diagrams of confined nitrogen in silica slit pores as a function of the pore width determined by the G–L coexisting cell method. Filled symbols represent the corresponding critical point

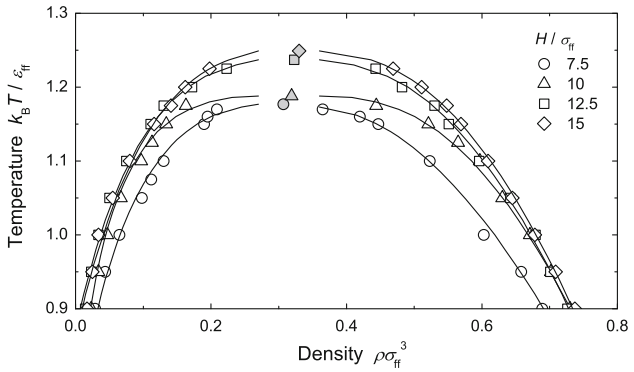

Fig. 3 Phase diagrams of confined nitrogen in fluid slit pores as a function of the pore width determined by the G–L coexisting cell method. Filled symbols represent the corresponding critical point

critical temperatures, $T_c^* = k_B T/\varepsilon_{ff}$, are plotted in Fig. 4 against the inverse reduced slit pore width, $1/w^* = \sigma_{ff}/w$. In this study, the slit pore width w was defined as the distance between the positions at which the solid–fluid interaction potential Φ becomes zero. In the case of the fluid slit pores, T_c^* linearly decreased from the reduced critical temperature (=1.3) of the bulk LJ fluid with decreasing slit pore width, which should be attributed to finite size effects. On the other hand, for the silica slit pores, the T_c^* value also decreased in a linear fashion; however, the slope was significantly larger than that for the fluid slit pores, which suggests that the finite size effects are more enhanced in the silica slit pores. Therefore, we defined the following effective pore width for the fluid confined in the silica slit pore:

$$w_{\mathrm{eff}}^* = w^* - 2w_{\mathrm{L}}^* \tag{4}$$

and determined the w_{L}^* value so that the slope of the T_c^* versus $1/w_{\mathrm{eff}}^*$ plot coincided with that of the T_c^* versus $1/w^*$ plot for the fluid slit pores. The obtained w_{L}^* value was 1.0, and this fact indicates that the first layers of the adsorbed molecules in contact with the pore walls act like a

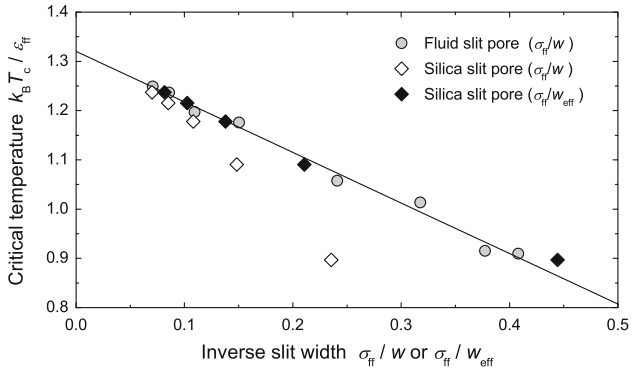

Fig. 4 Reduced critical temperatures of confined nitrogen in fluid and silica slit pores as a function of the inverse slit width. Solid linear line is the least-squares fit to the data of the fluid slit pores

"fluid wall" and impose extra finite size effects on the confined fluid in the central portion of the pore.

In this way, the T_c^* for the "fluid" pore gave a quite meaningful perspective for the role of confinement alone, on which the role of strong attraction in silica can be interpreted. Further studies are ongoing to establish a thermodynamic model that accounts not only for the pore size but also for the effects of the wall's attraction.

3 Characterization of nanopores based on a molecular simulation kernel

We recently developed the open pore cell Monte Carlo (MC) method to determine phase equilibria in nanopores (Miyahara and Tanaka 2013). The open pore cell MC method employs a pore cell with a "potential buffering field (PBF)," and combines it with a gas cell to measure the chemical potential of the system, as with the method introduced in the previous section. The pore cell is composed of two potential fields: a full potential field (FPF), in which a "full" interaction potential is exerted by the pore wall, and the PBF. The interaction potential in the PBF is continuously and linearly attenuated from the full potential value to zero, so that both ends of the pore cell are considered to be connected to an imaginary gas phase. The open pore cell MC method enables the precise estimation of the equilibrium chemical potential of the confined fluid with a *single* simulation, unlike the Peterson and Gubbins (1987) method or the gauge cell method. The low computational cost to evaluate the equilibrium chemical potential will allow us to construct kernels composed of adsorption isotherms by the GCMC method, which should be more precise than those obtained by NLDFT, to calculate the pore size distributions of porous materials.

In this study, to develop a kernel for the calculation of the pore size distribution (PSD) of activated carbons, we

Table 2 Parameters for the solid–fluid intermolecular potential

Wall	σ_{sf} (nm)	ε_{sf}/k (K)	ρ_s (nm^{-2})	Δ (nm)
Carbon	0.3494	52.42	114	0.335

assumed LJ nitrogen as adsorptive and carbon slit pores composed of two graphite slabs modeled by the Steele's 10-4-3 potential:

$$\phi(z) = 2\pi\rho_s\varepsilon_{sf}\sigma_{sf}^2\Delta\left[\frac{2}{5}\left(\frac{\sigma_{sf}}{z}\right)^{10} - \left(\frac{\sigma_{sf}}{z}\right)^{4} - \frac{\sigma_{sf}^4}{3\Delta(0.61\Delta + z)^3}\right] \quad (5)$$

The interaction parameters are tabulated in Table 2. The total interaction potential for a LJ nitrogen in the carbon slit pore of width H was calculated according to Eq. (3), and periodic boundary conditions were applied in the x and y directions.

We performed GCMC simulations to obtain the local adsorption isotherms of nitrogen in the carbon slit pores at 77 K, and also determined the equilibrium gas–liquid transition pressures for the respective carbon slit pores using the open pore cell MC method. The lateral dimensions of the simulation cell were set as $L_x^p = L_y^p = 10\ \sigma_{ff}$ for the GCMC method, and $L_x^p = 70\ \sigma_{ff}$ and $L_y^p = 10\ \sigma_{ff}$ for the open pore cell MC method, respectively. The FPF of the open pore cell MC method was placed at the center of the pore cell along the x direction with a length of 40 σ_{ff}, while the size of the gas cell was set to $L_x^g = L_y^g = L_z^g = 40\ \sigma_{ff}$. In the previous study (Miyahara and Tanaka 2013), we showed that the thickness of ca. $8\sigma_{ff}$ would be the lower limit for a stable liquid bridge in a carbon slit pore, and also that exactly the same equilibrium chemical potential can be obtained as long as two liquid menisci are within the FPF. The open pore cell MC method was applied in the range H = 2–10 nm in this study so that the thickness of the liquid bridge is at least lager than 20 σ_{ff} and also the two liquid menisci are within the FPF of 40 σ_{ff} in length. The length of the open pore cell of $L_x^p = 70\ \sigma_{ff}$ is suitable for maintaining such configuration. Further details of both the GCMC method and open pore cell MC method are given elsewhere (Miyahara and Tanaka 2013).

Figure 5 depicts the equilibrium gas–liquid transition pressures of nitrogen in the carbon slit pores at 77 K as a function of the slit width H obtained using the open pore cell MC method. We obtained the following analytical formula by fitting the simulation data in the range H = 2–10 nm:

$$H[\text{nm}] = 3.351\left[\frac{1.074}{0.01201 + ln(P_0/P)}\right]^{0.5465} + 0.0513 \quad (6)$$

Equation (6) was used to determine the equilibrium transition pressures for the respective local isotherms.

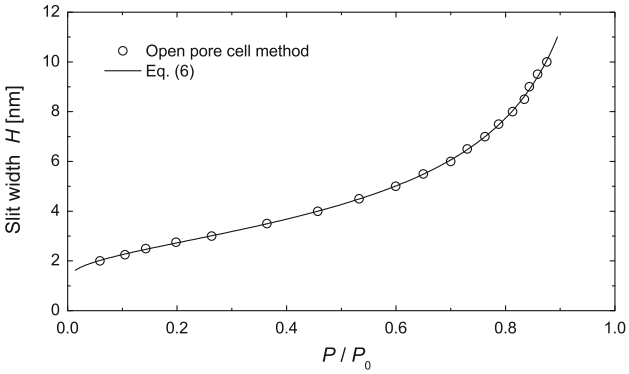

Fig. 5 Equilibrium gas–liquid transition pressures of nitrogen in carbon slit pores at 77 K as a function of the slit width H, obtained by the open pore cell MC method

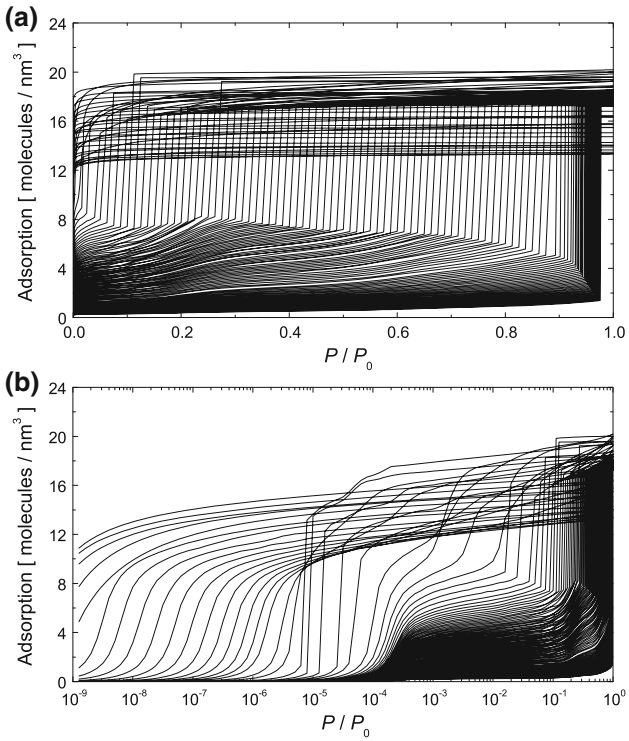

Fig. 6 GCMC kernel for nitrogen adsorption in carbon slit pores at 77 K developed in this study: (**a**) linear scale and (**b**) logarithmic scale

Then, as for the local isotherms on the carbon slit pores of H larger than 10 nm, the equilibrium transition pressures were taken from the data obtained by Tarazona's version of NLDFT (Tarazona 1985; Tarazona et al. 1987). Figure 6a, b show the GCMC kernel for the carbon slit pores developed in this study. The number of the local isotherms is 141, and the range of slit pore width w is 0.467–100 nm, where the definition of w is the same as that in the previous section.

Figure 7a, b represent the fittings of our GCMC kernel and the NLDFT kernel to the experimental nitrogen

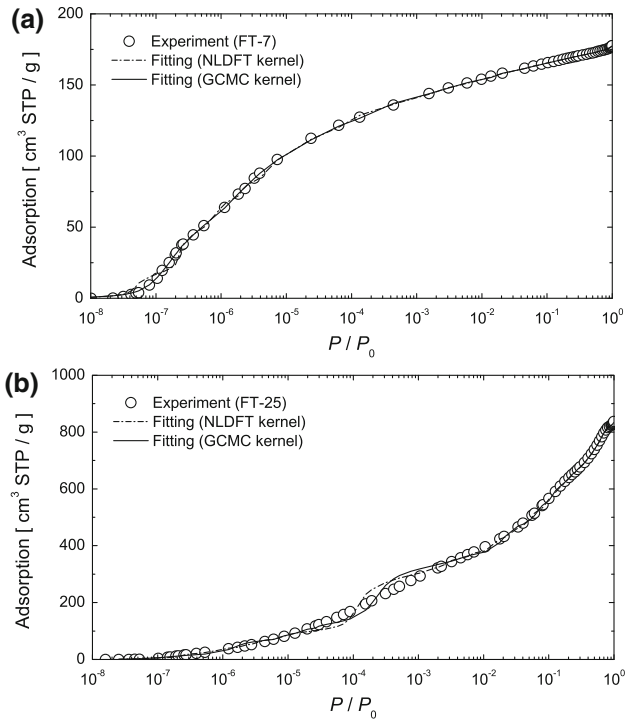

Fig. 7 Fittings of our GCMC kernel and the NLDFT kernel to the experimental nitrogen adsorption isotherms on activated carbons at 77 K: (**a**) FT-7 and (**b**) FT-25

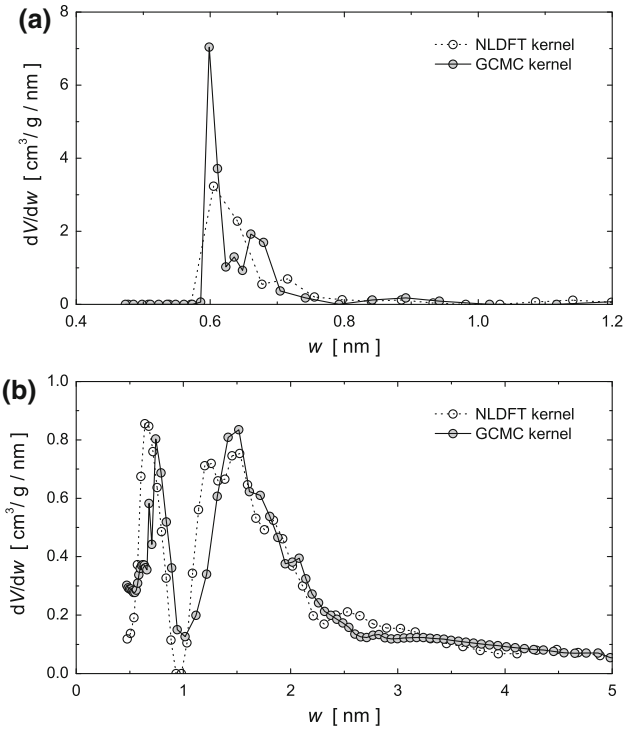

Fig. 8 PSDs derived from the fittings of our GCMC kernel and the NLDFT kernel to the experimental nitrogen adsorption isotherms on activated carbons at 77 K: (**a**) FT-7 and (**b**) FT-25

adsorption isotherms on the activated carbons (FT-7 and FT-25) at 77 K. The derived PSDs are shown in Fig. 8a, b. The Tikhonov regularization method with the L-curve criterion was used for solving the discrete ill-posed problems. The overall trends of the PSDs obtained from the GCMC kernel and the NLDFT kernel were nearly the same; however, an apparent difference could be seen for pore widths less than ca. $w = 1.0$ nm for both FT-7 and FT-25. This is likely due to the fact that the weighted density approximation used in NLDFT is not appropriate for small pores of molecular nitrogen size. Moreover, we notice that there is a considerable difference between the equilibrium transition pressures from the open pore cell MC method and NLDFT in the range $w = 2$–10 nm. This should also provide a difference between the PSDs from the GCMC kernel and the NLDFT kernel. Then, a prominent gap can be seen for both the PSDs of FT-25 from the GCMC kernel and the NLDFT kernel (Fig. 8b), which corresponds to a small kink in the fitted isotherms from the both kernels around $P/P_0 = 10^{-4}$ (Fig. 7b). This is because the local isotherms for carbon slit pores of $w = \sim 1$ nm with smooth pore walls have a sharp and large step in a low relative pressure region due to the micropore filling and such shape does not fit to the experimental adsorption isotherm showing a gradual uptake. Namely, it is the artificial gap originating from the pore model with infinitely wide parallel and smooth walls. Recently there has been an attempt to solve the problem by introducing surface roughness on the pore walls (Neimark et al. 2009).

Now, intensive calculations by our method with low calculation costs are ongoing to attain a cutting-edge characterization based on molecular simulation kernels with a variety of combinations of adsorbates, solids, and pore geometries. The new kernels are anticipated to be available soon.

4 Mechanism of adsorption-induced structural transition of stacked-layer PCP

We modeled a stacked-layer PCP simply by rigid layers and pillars located on the one side of the layers (Fig. 9). This simplified model should be a good description of ELM-11 (Li and Kaneko 2001; Kitaura et al. 2003; Noguchi et al. 2005; Kondo et al. 2006; Kanoh et al. 2009), which has a grid network formed by coordination bonds between metal ions and linker molecules and pillaring anions located on both sides of the grid network. The interlayer width for a closed state of the simplified model, $h_0 = 1.75\sigma_{\mathrm{ff}}$, was dominated by the length of the pillar. The interlayer widths for all the neighboring layers were assumed to always be the same during adsorption and desorption processes. LJ argon ($\sigma_{\mathrm{ff}} = 0.341$ nm and $\varepsilon_{\mathrm{ff}}/k = 119.8$ K) was used as the guest molecule, and the

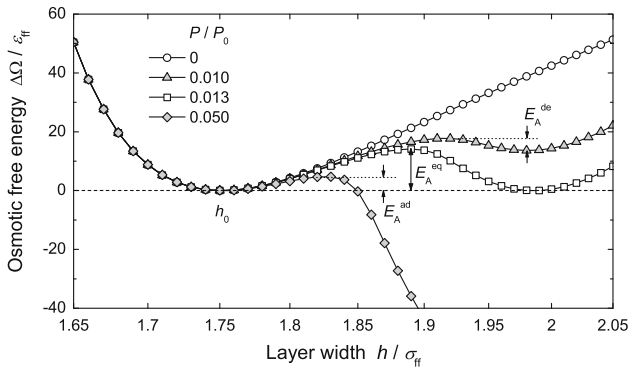

Fig. 9 Schematic representation of the stacked-layer PCP model

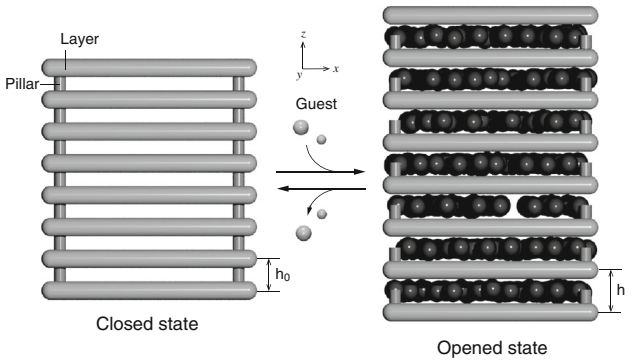

Fig. 10 Free energy changes as a function of the interlayer width of the stacked-layer PCP model for various bulk fluid pressures at $k_BT/\varepsilon_{ff} = 0.8$

stacked layers were modeled by the Steele's 10-4 potential composed of LJ carbon atoms ($\sigma_{ss} = 0.34$ nm and $\varepsilon_{ss}/k = 28$ K) with a density of $2.2\sigma_{ff}^{-2}$. The solid–fluid cross interaction parameters were obtained from the Lorentz-Berthelot mixing rules. The pillars had the same interaction parameters as the guests, and their density was set to $100\sigma_{ff}^{-2}$. A layer–layer interaction potential was obtained by an area integral of the Steele's 10-4 potential, and the total potential energy of the host framework was calculated as a sum of the layer–layer and pillar-layer interactions. Namely, the flexibility of the host framework is mainly controlled by attractive forces between the layers and repulsion forces between the layers and the pillars. The lateral dimensions of the simulation cell were set as $L_x = L_y = 10\sigma_{ff}$, and the height of the cell L_z was changed from $10.5\sigma_{ff}$ to $14.35\sigma_{ff}$. Periodic boundary conditions were applied for all directions. Further details of the simulation model are given elsewhere (Numaguchi et al. 2013).

The osmotic free energy change of the system during guest adsorption, Ω_{OS}, is obtained by the thermodynamic integration of the adsorption isotherm from the GCMC simulations as (Coudert et al. 2008; Numaguchi et al. 2013):

$$\Omega_{OS}(\mu, h) = F^{host}(h) + PV(h) - \int_{-\infty}^{\mu} d\mu' N(\mu', h) \tag{7}$$

where F^{host} is the Helmholtz free energy of the layers (host), P is the bulk pressure, $V(h)$ is the cell volume, and $N(\mu,h)$ represents the simulated adsorption isotherm on the host with the interlayer width h. The relative osmotic free energy for the change of the interlayer width from h_0 to h is given as:

$$\Delta\Omega_{OS}(\mu, h) = \Delta\Omega_{OS}(\mu, h) - \Delta\Omega_{OS}(\mu, h_0) \tag{8}$$

where change in the Helmholtz energy of the host, $\Delta F^{host}(h) = F^{host}(h) - F^{host}(h_0)$, which is contained in Eq. (8), was approximated to the change in the total potential energy of the host framework. This could be reasonable because the thermal fluctuation of the layer itself will change very little in this system upon the variation in the interlayer width, and thus, the term of the entropy change in $\Delta F^{host}(h)$ may be negligibly small.

Figure 10 shows the free energy changes as a function of the interlayer width for various bulk fluid pressures at $k_BT/\varepsilon_{ff} = 0.8$. At zero pressure, a global minimum appeared at $h = h_0$, and the free energy increased monotonically with increasing interlayer width due to the attractive forces working between the layers. The guest adsorption at $P/P_0 = 0.010$ provided a local minimum of the free energy at $h = 1.99\sigma_{ff}$ (metastable state). Then, at $P/P_0 = 0.013$, the free energy profile became bistable, which means that both states with interlayer widths of h_0 and $h = 1.99\sigma_{ff}$ are in thermodynamic equilibrium. A further increase in the pressure made the open state more stable, which suggests that the structural transition of the host is likely induced by adsorption of the guest under equilibrium conditions.

The aforementioned analysis was based on the theory of equilibrium; meanwhile, our free energy analysis method enables one to understand the kinetics of the adsorption-induced structural transition. Namely, if we assume 6 k_BT per layer as the energy fluctuation of the system, the equilibrium structural transition cannot be achieved because an energy barrier E_A^{eq}, existing between the two stable states, reaches 14.1 k_BT per layer. The energy barrier decreases with increasing relative pressure in the adsorption process, and finally, it coincides with the energy fluctuation of the system at $P/P_0 = 0.050$ (energy barrier E_A^{ad} in Fig. 10), which results in the spontaneous adsorption-induced structural transition of the system. On the other hand, in the desorption process, the energy barrier E_A^{de} for the transition from the open state to the closed state becomes the same with the energy fluctuation of the system at $P/P_0 = 0.010$, which is lower than the equilibrium structural transition pressure. This is the mechanism of the

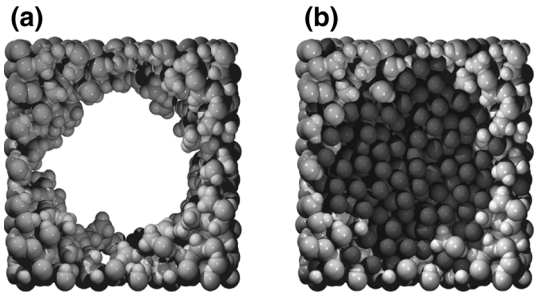

Fig. 11 Adsorption/desorption isotherm of argon on the stacked-layer PCP model at $k_BT/\varepsilon_{ff} = 0.8$

gate phenomenon with pronounced hysteresis, and the resulting adsorption/desorption isotherm at $k_BT/\varepsilon_{ff} = 0.8$ is shown in Fig. 11. The spontaneous structural transition pressure in the desorption process is significantly closer to the equilibrium structural transition pressure than that in the adsorption process, which should be a universal characteristic common to the adsorption-induced structural transitions in many PCPs.

The structural model of the PCP used in this study is quite simplified, but we must emphasize that the simplification itself enables us to analyze various factors separately to determine the "physical" essence of this complicated phenomenon.

5 Adsorption hysteresis in mesoporous silica with surface roughness

A bulk fused silica was constructed by the molecular dynamics method with the van Beest, Kramers, and van Santen (BKS)-type potential by quenching from 4,000 K to room temperature at a rate of 0.23 K/fs. The amorphous silica block was carved out to reproduce the experimentally determined electron density profile (EDP) of MCM-41 (Muroyama et al. 2006, 2008; Tanaka et al. 2013), and the resulting atomistic MCM-41 model is shown in Fig. 12. Adsorption isotherms of LJ argon on the MCM-41 model at 75 K and 80 K were obtained by the GCMC and gauge cell methods. The interaction parameters used in this study were $\sigma_{ff} = 0.341$ nm and $\varepsilon_{ff}/k_B = 119.8$ K for argon; and $\sigma_{O-O} = 0.2708$ nm, $\varepsilon_{O-O}/k_B = 101.6$ K, and $\sigma_{Si-Si} = 0.0677$ nm, $\varepsilon_{Si-Si}/k_B = 18.6$ K for silica. The solid–fluid cross interaction parameters were obtained by applying the Lorentz-Berthelot mixing rules. Further details for the model construction and the GCMC simulations are given elsewhere (Tanaka et al. 2013).

According to Neimark and Vishnyakov (2006), we calculated the canonical work function, $W(\mu,N)$, by integrating a sigmoid adsorption isotherm, $\mu_s(N)$, obtained from the gauge cell method:

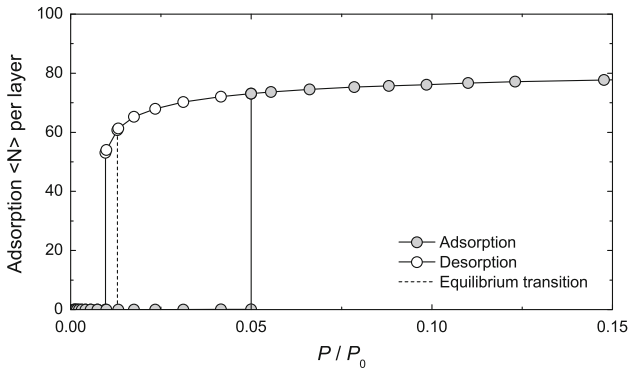

Fig. 12 Atomistic silica model obtained for reproducing the experimental electron density of MCM-41: (**a**) before adsorption and (**b**) after capillary condensation

$$W(\mu,N) = \int_{N_1}^{N_2} \mu_s(N')dN' - \mu N \tag{9}$$

Equation (9) provides the work required for a state change from a multilayer adsorption state (adsorption amount, N_1) to a capillary condensed state (adsorption amount, N_2) at a constant chemical potential μ.

Figure 13 shows a comparison between the simulated argon adsorption isotherms on the atomistic MCM-41 model and experimental argon isotherms at 75 K and 80 K. The MCM-41 model with proper surface roughness could reproduce the experimental data without any parameter adjustments. Moreover, thermodynamic equilibrium condensation pressures, P_{eq}, obtained from the simulations at respective temperatures were in qualitative agreement with the experimental desorption branches. Figure 14 depicts changes in the canonical work function, ΔW, with reference to W at point α. The ΔW value shows a local maximum between the minima of the α and β states; when the energy barrier $E_A(P_{eq})$ at the equilibrium transition pressure is larger than the energy fluctuation of the system, the gas–liquid transition cannot be achieved at this pressure. However, the energy barrier decreases with increasing pressure, and thus, spontaneous capillary condensation should occur when the energy barrier, $E_A(P_{ad})$, coincides with the energy fluctuation of the system. The $E_A(P_{ad})$ value obtained from a comparison between simulated and experimental data at 75 K was 2.1 k_BT per reduced length of the simulation box along the pore axis. We therefore assumed it as the energy fluctuation of the system, and predicted the spontaneous capillary condensation pressure P_{ad} at 80 K. It is obvious that the predicted P_{ad} value is in good agreement with experiment (see Fig. 13b). This fact strongly suggests that the adsorption branch with hysteresis for MCM-41 comes from spontaneous capillary condensation from a metastable state.

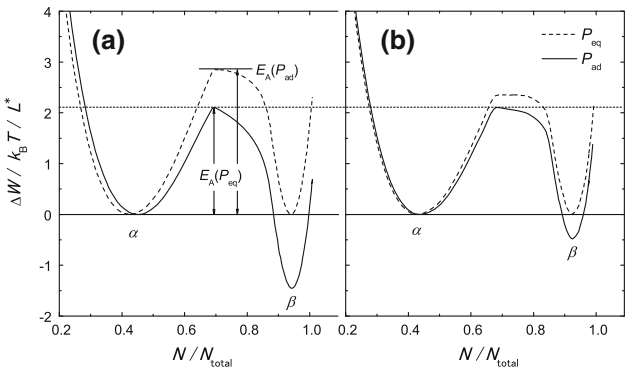

Fig. 13 Comparison of simulated argon adsorption isotherms on the atomistic MCM-41 model and experimental argon isotherms: (**a**) 75 K and (**b**) 80 K

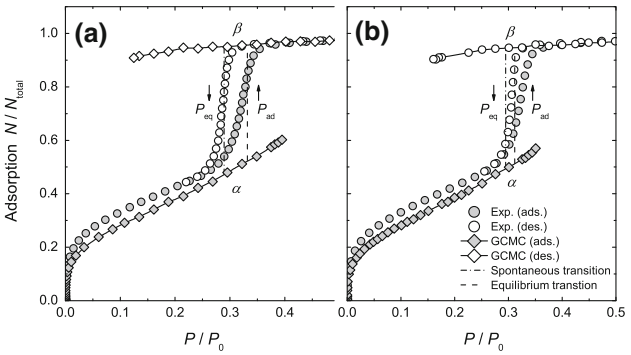

Fig. 14 Changes in the canonical work function, ΔW, with reference to W at point α: (**a**) 75 K and (**b**) 80 K. $L^* = L/\sigma_{ff}$, and L is the length of the simulation box along the pore axis

6 Conclusions

We investigated the critical properties of confined LJ fluids in silica and fluid pores using the G–L coexisting cell method. We found that the first layers of adsorbed molecules in contact with the attractive silica pore walls acted like a "fluid" wall, which resulted in the suppression of critical points. These findings can be applied in the development of a thermodynamic model for the critical behaviors of the confined fluids, and should be a useful tool for adsorption engineering.

We developed a new kernel for PSD analysis, consisting of local nitrogen adsorption isotherms in carbon slit pores at 77 K, by combining the GCMC method and the open pore cell method. We showed that overall trends of the PSDs of the activated carbons calculated with our new kernel and with the conventional NLDFT kernel were nearly the same; however, apparent difference was observed between them, which should be due to the approximations introduced into the NLDFT. We are now constructing kernels for various pore geometries (slit, cylindrical, and spherical), materials (carbon and silica), and adsorbates (nitrogen, argon, carbon dioxide, and so on) by the above-mentioned molecular simulation techniques in collaboration with BEL Japan Inc. And, BEL Japan Inc. is starting to distribute a software for the characterization of porous materials, "BELMaster," equipped with a part of our new kernels.

The free energy analysis method with the aid of GCMC simulations was applied to investigate the mechanism of the adsorption-induced structural transition observed in a stacked-layer PCP, based on both the theory of equilibrium and kinetics. The simplicity of the model used in this study as the PCP framework was beneficial because we could determine the "physical" essence of complicated phenomena. Our free energy analysis method provided a clear understanding of the adsorption-induced structural transitions in the stacked-layer PCP, and it might be extended to various soft PCPs by constructing a structure model with appropriate morphology. Therefore, the method may contribute to the rational design of PCPs for industrial application. Based on the understanding provided by our simple model, we are now performing atomistic molecular simulations to determine the key factors in more complex systems.

We constructed an atomistic silica pore model that mimicked MCM-41 with realistic surface roughness, and performed molecular simulations to understand the capillary condensation mechanism with adsorption hysteresis. The inspection of the canonical work function suggested that the adsorption branch with hysteresis for MCM-41 arose from spontaneous capillary condensation from a metastable state. Our methodology for molecular modeling of the capillary condensation in siliceous mesoporous materials should be useful for elucidating the dissipation mechanism of the adsorption hysteresis in MCM-41 with small mesopores (less than ca. 3 nm) for nitrogen adsorption at 77 K and argon adsorption at 87 K; these studies are now in progress.

We sincerely hope that the development and application of these molecular simulations, together with experimental findings, will further serve as powerful tools for determining the physical bases of various complicated phenomena, and find practical use industrially.

Acknowledgments The authors are grateful to Mr. Funahashi, Mr. Fukuoka, and Mr. Harada for their assistance in this work. This work was financially supported by the "Development of Advanced Measurement and Analysis Systems" Project of the Japan Science and Technology Agency (JST), and a Grant-in-Aid for Scientific Research (B) 24360318 from MEXT.

References

Coasne, B., Di Renzo, F., Galarneau, A., Pellenq, R.J.M.: Adsorption of simple fluid on silica surface and nanopore: effect of surface chemistry and pore shape. Langmuir **24**, 7285–7293 (2008a)

Coasne, B., Galarneau, A., Di Renzo, F., Pellenq, R.J.M.: Effect of morphological defects on gas adsorption in nanoporous silicas. J. Phys. Chem. C **111**, 15759–15770 (2007)

Coasne, B., Galarneau, A., Di Renzo, F., Pellenq, R.J.M.: Gas adsorption in mesoporous micelle-templated silicas: MCM-41, MCM-48, and SBA-15. Langmuir **22**, 11097–11105 (2006a)

Coasne, B., Galarneau, A., Di Renzo, F., Pellenq, R.J.M.: Molecular simulation of adsorption and intrusion in nanopores. Adsorption **14**, 215–221 (2008b)

Coasne, B., Galarneau, A., Di Renzo, F., Pellenq, R.J.M.: Molecular simulation of nitrogen adsorption in nanoporous silica. Langmuir **26**, 10872–10881 (2010)

Coasne, B., Galarneau, A., Pellenq, R.J.M., Di Renzo, F.: Adsorption, intrusion and freezing in porous silica: the view from the nanoscale. Chem. Soc. Rev. **42**, 4141–4171 (2013)

Coasne, B., Hung, F.R., Pellenq, R.J.M., Siperstein, F.R., Gubbins, K.E.: Adsorption of sample gases in MCM-41 materials: The role of surface roughness. Langmuir **22**, 194–202 (2006b)

Coasne, B., Pellenq, R.J.M.: A grand canonical Monte Carlo study of capillary condensation in mesoporous media: Effect of the pore morphology and topology. J. Chem. Phys. **121**, 3767–3774 (2004a)

Coasne, B., Pellenq, R.J.M.: Grand canonical Monte Carlo simulation of argon adsorption at the surface of silica nanopores: effect of pore size, pore morphology, and surface roughness. J. Chem. Phys. **120**, 2913–2922 (2004b)

Coasne, B., Ugliengo, P.: Atomistic model of micelle-templated mesoporous silicas: structural, morphological, and adsorption properties. Langmuir **28**, 11131–11141 (2012)

Coudert, F.-X., Jeffroy, M., Fuchs, A.H., Boutin, A., Mellot-Draznieks, C.: Thermodynamics of guest-induced structural transitions in hybrid organic-inorganic frameworks. J. Am. Chem. Soc. **130**, 14294–14302 (2008)

Do, D.D., Do, H.D.: Pore characterization of carbonaceous materials by DFT and GCMC simulations: a review. Adsorpt. Sci. Tech. **21**, 389–423 (2003)

Düren, T., Sarkisov, L., Yaghi, O.M., Snurr, R.Q.: Design of new materials for methane storage. Langmuir **20**, 2683–2689 (2004)

Düren, T., Snurr, R.Q.: Assessment of isoreticular metal–organic frameworks for adsorption separations: a molecular simulation Study of methane/*n*-butane mixtures. J. Phys. Chem. B **108**, 15703–15708 (2004)

Gelb, L.D., Gubbins, K.E., Radhakrishnan, R., Sliwinska-Bartkowiak, M.: Phase separation in confined systems. Rep. Prog. Phys. **62**, 1573–1659 (1999)

Gubbins, K.E., Liu, Y.-C., Moore, J.D., Palmer, J.C.: Molecular modeling of matter: impact and prospects in engineering. Ind. Eng. Chem. Res. **49**, 3026–3046 (2010)

Gubbins, K.E., Liu, Y.-C., Moore, J.D., Palmer, J.C.: The role of molecular modeling in confined systems: impact and prospects. Phys. Chem. Chem. Phys. **13**, 58–85 (2011)

Horcajada, P., Serre, C., Vallet-Regi, M., Sebban, M., Taulelle, F., Ferey, G.: Metal–organic frameworks as efficient materials for drug delivery. Angew. Chem. Int. Ed. **45**, 5974–5978 (2006)

Horike, S., Shimomura, S., Kitagawa, S.: Soft porous crystals. Nat. Chem. **1**, 695–704 (2009)

Jagiello, J., Olivier, J.P.: 2D-NLDFT adsorption models for carbon slit-shaped pores with surface energetical heterogeneity and geometrical corrugation. Carbon **55**, 70–80 (2013)

Jana, S., Singh, J.K., Kwak, S.K.: Vapor-liquid critical and interfacial properties of square-well fluids in slit pores. J. Chem. Phys. **130**, 214707 (2009)

Kanda, H., Miyahara, M., Higashitani, K.: Triple point of Lennard-Jones fluid in slit nanopore: solidification of critical condensate. J. Chem. Phys. **120**, 6173–6179 (2004)

Kanda, H., Miyahara, M.: Sublimation phenomena of Lennard-Jones fluids in slit nanopores. J. Chem. Phys. **126**, 054703 (2007)

Kanoh, H., Kondo, A., Noguchi, H., Kajiro, H., Tohdoh, A., Hattori, Y., Xu, W.-C., Inoue, M., Sugiura, T., Morita, K., Tanaka, H., Ohba, T., Kaneko, K.: Elastic layer-structured metal organic frameworks (ELMs). J. Colloid Interface Sci. **334**, 1–7 (2009)

Kitagawa, S., Kitaura, R., Noro, S.: Functional porous coordination polymers. Angew. Chem. Int. Ed. **43**, 2334–2375 (2004)

Kitaura, R., Seki, K., Akiyama, G., Kitagawa, S.: Porous coordination-polymer crystals with gated channels specific for supercritical gases. Angew. Chem. Int. Ed. **42**, 428–431 (2003)

Kondo, A., Noguchi, H., Ohnishi, S., Kajiro, H., Tohdoh, A., Hattori, Y., Xu, W.-C., Tanaka, H., Kanoh, H., Kaneko, K.: Novel expansion/shrinkage modulation of 2D layered MOF triggered by clathrate formation with CO_2 molecules. Nano Lett. **6**, 2581–2584 (2006)

Li, D., Kaneko, K.: Hydrogen bond-regulated microporous nature of copper complex-assembled microcrystals. Chem. Phys. Lett. **335**, 50–56 (2001)

Liu, Y., Panagiotopoulos, A.Z., Debenedetti, P.G.: Finite-size scaling study of the vapor-liquid critical properties of confined fluids: crossover from three dimensions to two dimensions. J. Chem. Phys. **132**, 144107 (2010)

Miyahara, M., Gubbins, K.E.: Freezing/melting phenomena for Lennard-Jones methane in slit pores: a Monte Carlo study. J. Chem. Phys. **106**, 2865–2880 (1997)

Miyahara, M., Kanda, H., Shibao, M., Higashitani, K.: Solid-liquid phase transition of Lennard-Jones fluid in slit pores under tensile condition. J. Chem. Phys. **112**, 9909–9916 (2000a)

Miyahara, M., Kanda, H., Yoshioka, T., Okazaki, M.: Modeling capillary condensation in cylindrical nanopores: a molecular dynamics study. Langmuir **16**, 4293–4299 (2000b)

Miyahara, M., Yoshioka, T., Okazaki, M.: Determination of adsorption equilibria in pores by molecular dynamics in a unit cell with imaginary gas phase. J. Chem. Phys. **106**, 8124–8134 (1997)

Miyahara, M.T., Tanaka, H.: Determination of phase equilibria in confined systems by open pore cell Monte Carlo method. J. Chem. Phys. **138**, 084709 (2013)

Mon, K.K., Binder, K.: Finite size effects for the simulation of phase coexistence in the Gibbs ensemble near the critical point. J. Chem. Phys. **96**, 6989–6995 (1992)

Muroyama, N., Ohsuna, T., Ryoo, R., Kubota, Y., Terasaki, O.: An analytical approach to determine the pore shape and size of MCM-41 materials from X-ray diffraction data. J. Phys. Chem. B **110**, 10630–10635 (2006)

Muroyama, N., Yoshimura, A., Kubota, Y., Miyasaka, K., Ohsuna, T., Ryoo, R., Ravikovitch, P.I., Neimark, A.V., Takata, M., Terasaki, O.: Argon adsorption on MCM-41 mesoporous crystal studied by in situ synchrotron powder X-ray diffraction. J. Phys. Chem. C **112**, 10803–10813 (2008)

Nakagawa, K., Tanaka, D., Horike, S., Shimomura, S., Higuchi, M., Kitagawa, S.: Enhanced selectivity of CO_2 from a ternary gas mixture in an interdigitated porous framework. Chem. Commun. **46**, 4258–4260 (2010)

Neimark, A.V., Lin, Y., Ravikovitch, P.I., Thommes, M.: Quenched solid density functional theory and pore size analysis of micro-mesoporous carbons. Carbon **47**, 1617–1628 (2009)

Neimark, A.V., Vishnyakov, A.: Gauge cell method for simulation studies of phase transitions in confined systems. Phys. Rev. E **62**, 4611–4622 (2000)

Neimark, A.V., Vishnyakov, A.: Phase transitions and criticality in small systems: Vapor-liquid transition in nanoscale spherical cavities. J. Phys. Chem. B **110**, 9403–9412 (2006)

Noguchi, H., Kondo, A., Hattori, Y., Kanoh, H., Kajiro, H., Kaneko, K.: Clathrate-formation mediated adsorption of methane on Cu-complex crystals. J. Phys. Chem. B **109**, 13851–13853 (2005)

Numaguchi, R., Tanaka, H., Watanabe, S., Miyahara, M.T.: Simulation study for adsorption-induced structural transition in stacked-layer porous coordination polymers: Equilibrium and hysteretic adsorption behaviors. J. Chem. Phys. **138**, 054708 (2013)

Olivier, J.P.: Modeling physical adsorption on porous and nonporous solids using density functional theory. J. Porous Mater. **2**, 9–17 (1995)

Peterson, B.K., Gubbins, K.E.: Phase-transitions in a cylindrical pore—grand canonical Monte-Carlo, mean field-theory and the Kelvin equation. Mol. Phys. **62**, 215–226 (1987)

Ravikovitch, P.I., Haller, G.L., Neimark, A.V.: Density functional theory model for calculating pore size distributions: pore structure of nanoporous catalysts. Adv. Colloid Interface Sci. **76**, 203–226 (1998)

Ravikovitch, P.I., Odomhnaill, S.C., Neimark, A.V., Schuth, F., Unger, K.K.: Capillary hysteresis in nanopores: theoretical and experimental studies of nitrogen adsorption on MCM-41. Langmuir **11**, 4765–4772 (1995)

Ravikovitch, P.I., Vishnyakov, A., Neimark, A.V.: Density functional theories and molecular simulations of adsorption and phase transitions in nanopores. Phys. Rev. E **64**, 011602 (2001)

Ravikovitch, P.I., Vishnyakov, A., Russo, R., Neimark, A.V.: Unified approach to pore size characterization of microporous carbonaceous materials from N_2, Ar, and CO_2 Adsorption Isotherms. Langmuir **16**, 2311–2320 (2000)

Rosseinsky, M.J.: Recent developments in metal–organic framework chemistry: design, discovery, permanent porosity and flexibility. Microporous Mesoporous Mater. **73**, 15–30 (2004)

Rowsell, J.L.C., Yaghi, O.M.: Metal–organic frameworks: a new class of porous materials. Microporous and Mesoporous Mater. **73**, 3–14 (2004)

Shi, W., Zhao, X., Johnson, J.K.: Phase transitions of adsorbed fluids computed from multiple-histogram reweighting. Mol. Phys. **100**, 2139–2150 (2002)

Singh, S.K., Singh, J.K.: Effect of pore morphology on vapor-liquid phase transition and crossover behavior of critical properties from 3D to 2D. Fluid Phase Equilib. **300**, 182–187 (2011)

Sonwane, C.G., Jones, C.W., Ludovice, P.J.: A model for the structure of MCM-41 incorporating surface roughness. J. Phys. Chem. B **109**, 23395–23404 (2005)

Sugiyama, H., Watanabe, S., Tanaka, H., Miyahara, M.T.: Adsorption-induced structural transition of an interpenetrated porous coordination polymer: Detailed exploration of free energy profiles. Langmuir **28**, 5093–5100 (2012)

Tanaka, H., Hiratsuka, T., Nishiyama, N., Mori, K., Miyahara, M.T.: Capillary condensation in mesoporous silica with surface roughness. Adsorption **19**, 631–641 (2013)

Tarazona, P., Marconi, U.M.B., Evans, R.: Phase-equilibria of fluid interfaces and confined fluids—nonlocal versus local density functionals. Mol. Phys. **60**, 573–595 (1987)

Tarazona, P.: Free-energy density functional for hard-spheres. Phys. Rev. A **31**, 2672–2679 (1985)

Vishnyakov, A., Piotrovskaya, E.M., Brodskaya, E.N., Votyakov, E.V., Tovbin Yu, K.: Critical properties of Lennard-Jones fluids in narrow slit-shaped pores. Langmuir **17**, 4451–4458 (2001)

Watanabe, S., Sugiyama, H., Adachi, H., Tanaka, H., Miyahara, M.T.: Free energy analysis for adsorption-induced lattice transition of flexible coordination framework. J. Chem. Phys. **130**, 164707 (2009)

Yanai, N., Kitayama, K., Hijikata, Y., Sato, H., Matsuda, R., Kubota, Y., Takata, M., Mizuno, M., Uemura, T., Kitagawa, S.: Gas detection by structural variations of fluorescent guest molecules in a flexible porous coordination polymer. Nat. Mater. **10**, 787–793 (2011)